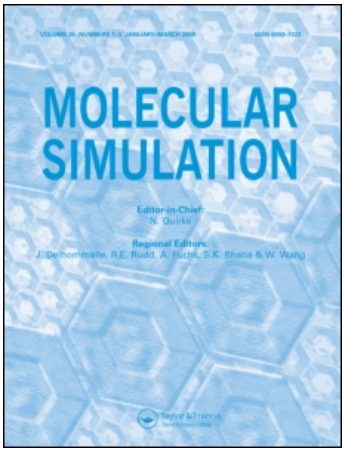

Molecular Simulation
Publication details, including instructions for authors and subscription information:
http://www.informaworld.com/smpp/title~content=t713644482

Structural Properties of Stage-2 Alkali-Metal Graphite Interclation Compounds

Tahir Çain[ab]; Surajit Sen[c]; Hyangsuk Seong[c]; S. D. Mahanti[c]
[a] Molecular Simulations Inc, Pasadena, CA [b] Beckman Institute, California Institute of Technology, Pasadena, CA [c] Department of Physics and Astronomy and Center for Fundamental Materials Research, Michigan State University, East Lansing, MI

To cite this Article Çain, Tahir , Sen, Surajit , Seong, Hyangsuk and Mahanti, S. D.(1993) 'Structural Properties of Stage-2 Alkali-Metal Graphite Interclation Compounds', Molecular Simulation, 10: 1, 41 — 59
To link to this Article: DOI: 10.1080/08927029308022497
URL: http://dx.doi.org/10.1080/08927029308022497

Molecular Simulation, 1993, Vol. 10(1), pp. 41–59
Reprints available directly from the publisher
Photocopying permitted by license only

STRUCTURAL PROPERTIES OF STAGE-2 ALKALI-METAL GRAPHITE INTERCLATION COMPOUNDS: A MOLECULAR DYNAMICS STUDY

TAHIR ÇAĞIN*, SURAJIT SEN†, HYANGSUK SEONG†
AND S.D. MAHANTI†

**Molecular Simulations Inc, 199 S. Robles Ave, Suite 540, Pasadena, CA 91101*
and Beckman Institute, California Institute of Technology, Pasadena, CA 91125
†Department of Physics and Astronomy
and Center for Fundamental Materials Research,
Michigan State University, East Lansing, MI 48824-1116

(Received June 1992, accepted July 1992)

An extensive study on low temperature solid and high temperature liquid phases of stage 2 alkali-metal graphite intercalation compounds (GICs), as examples of two dimensional screened Coulomb (repulsive) systems on strongly corrugation modulated substrates, is presented using constant energy and constant temperature (Nosé) Molecular Dynamics (MD) simulations. We present pair correlation functions, static structure factors and snapshots of microscopic structures in the liquid phase, in the freezing region and in the solid phase. Average energy, diffusion constant and the number of disclinations are monitored as a function of temperature to track down the transition (freezing) region. We also find that the number density of the topological defects (such as dislocations and disclinations) decreases rapidly at the freezing transition. In the solid phase of RbC_{24} we find small triangular domains of $(\sqrt{7}\times\sqrt{7})$ Rb structure with welldefined domain walls consisting of (2×2) and $(2\times3\times\sqrt{7})$ elemental plaquettes of Rb. These nanostructures provide a clear picture of the discommensurations (domain walls) and a consistent understanding of the X-ray diffraction measurements. Our simulation studies suggest a Periodic Domain Wall model to describe the low temperature solid phase structure of the alkali metal GIC's. This model explains the dominant features of the experimental X-ray structure factor.

KEY WORDS: Graphite Intercalation Compounds, Two dimensional melting/freezing, Screened Coulomb interactions, Molecular Dynamics, Domains, Structure Factor

INTRODUCTION

Graphite intercalation compounds (GIC's) [1], adsorbed monolayers [2] and reconstructed surfaces [3] represent a class of systems with competing interactions which are of considerable interest in condensed matter physics. Structural properties of binary and ternary GIC's have attracted particular attention over the past decade [4]. While many of the interesting physical properties of these systems are now well understood, a detailed microscopic understanding of the incommensurability of stage n ($n \geq 2$) GIC's containing K, Rb and Cs as intercalants is still lacking. A careful study of the microscopic structure of the alkali-metal GIC's using Molecular Dynamics (MD) simulations is the main purpose of this work.

Stage-n GIC's are characterized by a stacking sequence of graphite and intercalant layers in which neighbouring intercalant layers are separated by n

graphitic layers [4, 5]. The intercalant ions interact essentially via screened Coulomb repulsion [6] and feel an effective one particle corrugation potential produced by the graphite substrate [6–8]. The coupling between the intercalant ions in the different layers is small [9] in GIC's with $n \geq 2$ thereby making these systems strongly two dimensional. These systems embody competition between (a) *two length scales*, and (b) *two energy scales*. The former arises due to the spatial periodicity of the corrugation potential and the average separation between the intercalant ions while the latter relates to the depth of the corrugation potential and the interaction energy per ion. Both of these are controlled by the *density of the intercalant ions per carbon*. As we shall see in Section 5, the density plays a crucial role in determining the structure of the GIC's.

The main goal of this work is to use the available interatomic potentials to study the *real* and *κ-space structures* of stage-2 alkali metal GIC's *in liquid* and *solid phases*. In particular, we study the RbC_{24} GIC whose room temperature (liquid phase) static and dynamic structure factors have been studied in considerable detail recently [6–8, 10–12]. Good agreement with experimental results have been obtained in these studies using simple two body screened Coulomb potentials between Rb ions and an external corrugation potential to describe the substrate [6, 7, 10–12]. Earlier integral equation studies and MD simulation results as well as our present study (with the largest system being an 864 ion system) show that the RbC_{24} system behaves like a highly corrugation modulated liquid at $300\,K > T > 200\,K$. A brief account of this work has been recently published [13].

A plot of energy versus temperature reveals a well defined finite slope, dT/dE, in the temperature regime $240\,K > T > 180\,K$, distinct from the slopes at higher and lower temperatures, indicating a liquid to solid freezing transition. In this transition region the diffusion constant and the density of disclinations (topological defects) change dramatically with temperature. The transition appears to be continuous although a weak first order transition is not inadmissible within the accuracy of our calculations.

The solid phase exhibits small domains of $(\sqrt{7} \times \sqrt{7} \times \sqrt{7})$) Rb structure with domain walls consisting of $(2 \times 2 \times 2)$ and $(2 \times 3 \times \sqrt{7})$ elemental placquets of Rb. We will show that these *nano-structures* provide an excellent understanding of the dominant features of the experimentally obtained X-ray structure factors [14].

This paper is organized as follows. Section 2 gives the details of the MD simulation studies. Section 3 presents our studies on the liquid phase of the stage 2 GIC's and Section 4 presents our results for the freezing region. Section 5 focusses on the solid phase of the stage 2 GIC's. Finally in Section 6 we summarize our results.

2 MODEL AND METHOD

Recent MD studies on the liquid state structure and dynamics of the RbC_{24} stage-2 GIC have obtained an excellent agreement with experiments [6, 10, 12–17]. We therefore use the potential model used for these earlier calculations to study the liquid to solid freezing and the structure of the solid phase. The Rb ions are assumed to interact via the following two body repulsive potential [6],

$$V^{(2)}(r_1, r_2) = q^2 \exp(-\theta |r_1 - r_2|)/|r_1 - r_2|, \tag{2.1}$$

where $q = 4.8028 \times 10^{-10}$ esu and $\theta = 0.49\,\text{Å}^{-1}$. It may be noted that the above potential is a realistic potential for intercalation compounds where the intercalants

are charged objects. What makes the simulation considered in this work especially interesting is that screened Coulomb systems, such as the one treated here, are significantly more difficult to handle in simulations studies (due to the exponential form of the interaction) than the Lennard-Jones and other (algebraic) "short range" systems. Recently, Robbins *et al.* have carried out a MD study of the static properties of three dimensional screened Coulomb systems [18].

As mentioned earlier, the graphite substrate is represented by a rigid one—body graphite corrugation potential [6–8] which is chosen to be

$$V^{(1)}(r) = 2K\{2\cos(2\pi x/a)\cos(2\pi y/\sqrt{3}a) + \cos(4\pi y/\sqrt{3}a)\}, \qquad (2.2)$$

with $K = -0.45$ in reduced units, extrapolated from experiement, such that $2K/k_B \equiv -270\,K$, k_B being the Boltzmann constant. The constant $a = 2.46\,Å$ is the distance between the centers of the nearest neighbor graphite hexagons. The structure and dynamics of interacting many body systems on one-body corrugation potentials is a subject of strong interest on which little appears to be known at the present time [19, 20]. Interestingly, many body systems on corrugation modulated surfaces are also important to the understanding of structural transitions in solids [21, 22] and perhaps toward the understanding of the stability of granular systems [23] and of depinning of charge density waves [24].

It may be noted that the corrugation modulations described by equation (2.2) lies in the "intermediate strength" regime. To appreciate this point observe that the barrier height between the center of the graphite hexagons (where $V^{(1)}(r)$ have its minima) and the center of its bridge, which forms a saddle point (maxima of the potential are at the vertices of the hexagons) is 1080 K. The room temperature regime is typically ¼–⅓ of this barrier height. The physical system in this temperature regime therefore concerns repelling ions in an "intermediate" strength corrugation potential, a regime distinctly different from the well studies weak corrugation [25, 26] and strong corrugation (ie, lattice-gas like) regimes [27]. In addition, the wavelength of the corrugation potential is typically r ($\sqrt{3} \leqslant r \leqslant \sqrt{7}$) times smaller than the periodicity of the system in the absence of the corrugation potential.

The simulations are performed with 216 and 864 Rb ions distributed to ensure a planar density of 12 C's/Rb, i.e., 0.0318 ions/Å^2. The cell edges are arranged to lie on the fixed corrugation minima and periodic boundary conditions are imposed. The MD simulations are done on a Convex C240 machine using sixth order Gear predictor-corrector algorithm [28] to solve the Newtonian equations. The time step is taken to be 0.0028 picoseconds (ps) and equilibrium times of at least 350 ps for the 216 ion system and about 1 nanosecond (ns) for the 864 ions system are allowed. The energy per ion is conserved to 99.994% accuracy over the entire run periods for the 216 ion systems. The range of the two body potential is kept within a circle of radius 27.06 Å centered on any Rb. The results remain unaffected when a larger cut off radius is used.

The simulations reported in this paper are carried out in the temperature range $240\,K \leqslant T \leqslant 290\,K$ of the liquid phase; in the range $180\,K \leqslant T \leqslant 240\,K$, which we define as the "freezing or transition region" and then in the solid phase down to temperatures as low as 3 K. The system is initially heated up from an assumed structure and melted, equilibrated and then slowly cooled in steps of 10 K with long equilibration runs, typically exceeding 1 ns, for 864 ion system at each temperature when away from the transition region and −1.5 ns in the transition region. For the 216 ion system we have carried out both sytematic cooling and heating runs. For the

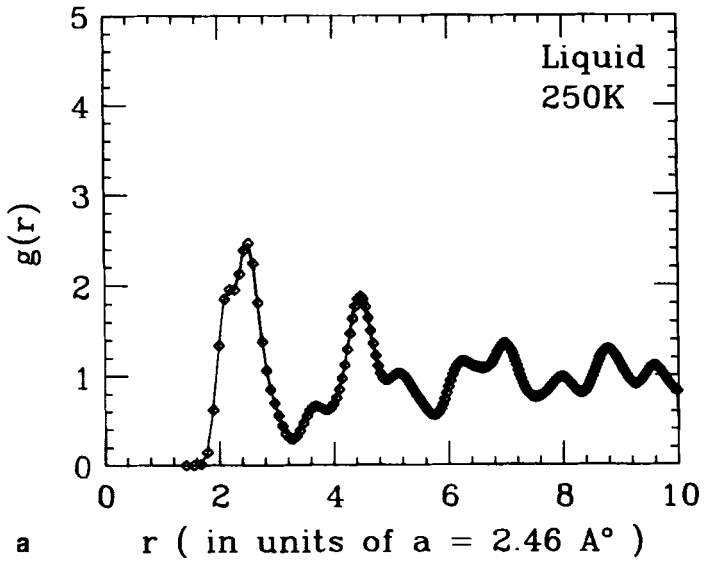

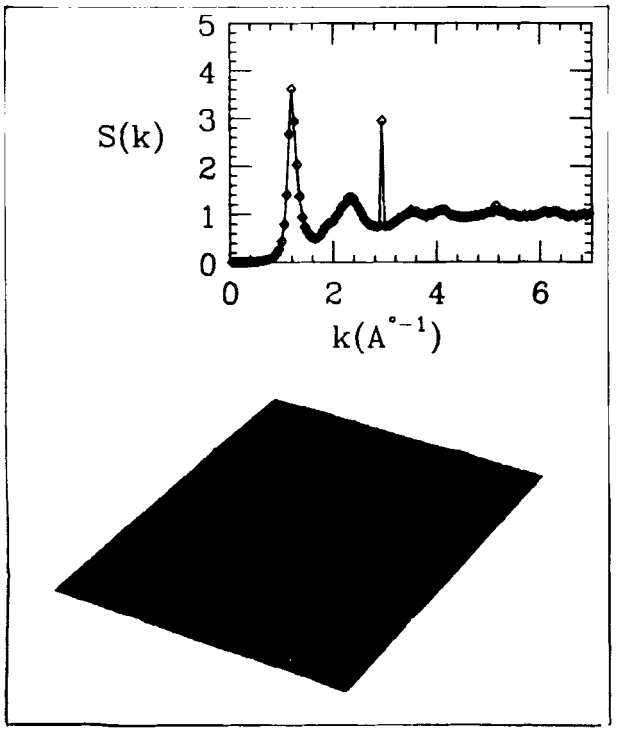

Figure 1 (a) Pair distribution function of the RbC_{24} system in the liquid phase at 250 K. (b) The anisotropic structure factor S(k) of the RbC_{24} system in the liquid phase at 250 K; Inset gives the circularly averaged S(k).

larger (864 ion) system we will discuss mainly our cooling runs which are well equilibrated. We have used both microcanonical (EVN) and canonical (TVN) ensembles for our MD simulations. The latter has been carried out using the standard Nosé algorithm [29]. As we shall see below, the results obtained via microcanonical and canonical ensemble simulations are excellent agreement with each other, thereby indicating that thermal equilibrium is reached at all temperatures.

3 LIQUID PHASE

As mentioned in Section 2, the structure and dynamics of the liquid phase at room temperature has been recently studied via integral equations and MD simulations [6–8, 10–12]. Our liquid state calculations check the correctness of our simulations against these results and provide a way to approach the solid phase.

We first present our calculations of the circularly averaged pair distribution function defined as follows,

$$g(r) \equiv (A/N^2)\left\langle \sum_i \sum_{i \neq j} \delta(r - r_{ij}(t)) \right\rangle, \tag{3.1}$$

where A is the area of the MD cell, N is the number of Rb ions in the cell and the angular brackets in (3.1) imply a time average. Figure 1a shows a plot of g(r) vs. r at T = 250 K for an 864 ion Rb system. Observe that g(r) appears significantly more structured than that of a pure liquid [28] where the first peak is usually a single peak. The liquid state of Rb is therefore strongly perturbed by the substrate. The shoulder at $2 \sim 2a$ in the first peak in Figure 1a suggests the presence of a second local length scale in addition to that represented by the dominant peak at $\sqrt{6}a < r = 2.53a < \sqrt{7}a$, where $\sqrt{6}a$ is the nominal distance between ions in the absence of corrugation for the chosen concentration (RbC_{24}, has a layer stoichiometry RbC_{12}, i.e., 12 Carbon atoms/Rb; area/Rb = $6a^2$). The absence of a single well defined peak already suggests the presence of multiple nearest neighbor distances even in the liquid state. As we shall see in Section 5, the lowering of the temperature leads to the appearance of multiple peaks emerging from the dominant first peak in Figure 1a.

The static structure factor S(k) is defined as follows,

$$S(k) = (1/N)\left\langle \left| \sum_i \exp i\mathbf{k} \cdot \mathbf{r}_i(t) \right|^2 \right\rangle, \tag{3.2}$$

where $r_i(t)$ is the position of the ith atom at time t. The circularly averaged static structure factor $S(|k|)$ is given in the inset in Figure 1b. The results are in excellent agreement with those of Chen *et al.* [6] The dominant peak at $k = 1.2\ \text{Å}^{-1}$ corresponds to the length scale of the dominant peak in Figure 1a. The sharp peak near $k = 3\ \text{Å}^{-1}$ corresponds to the length scale of the graphite unit cell and arises due to the strong perturbation of the intercalant fluid by the graphite corrugation potential. The anisotropic structure factor S(k), given in Figure 1b is in agreement with the previous work [6, 8, 10]. It has been discussed in detail in these references and will hence not be addressed here.

A snapshot of the liquid phase of RbC_{24} showing the locations of the Rb ions reveals a structure that is rich in topological defects where Rb ions are in five and seven fold nearest neighbor coordinations (i.e., disclinations and dislocation lines)

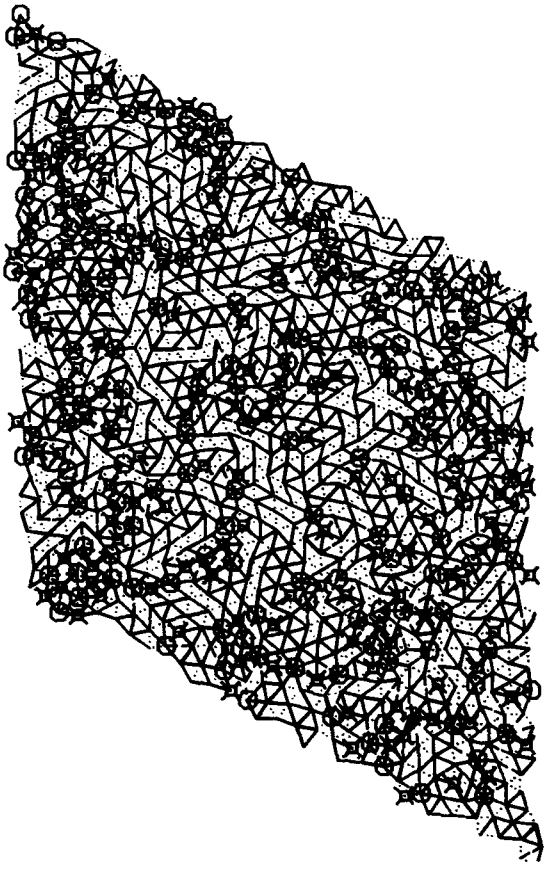

Figure 2 Picture of the 864 ion system in liquid phase at 250 K. Diamonds with 4 tails and circles mark the 5 and 7 fold coordinations, respectively. Solid lines connect Rb ions $\approx \sqrt{7}a$ apart while dot-dash and dotted lines connect ions $\approx 3a$ and $\approx 2a$ apart, respectively. (See Colour Plates)

as shown in Figure 2 [30–32]. The nearest neighbour bonds and the polygons in Figure 2 (and the rest of the paper) have been constructed using Voronoi construction [33].

Our present calculations (i.e., the well defined peaks in Figures 1a and 1b) and the picture of the lattice in Figure 2 suggest that the positions of the Rb ions in the liquid state are affected by the strong corrugation potential. Figures 2 and 3 present the number and the distribution of topological defects in the 864 ion system at $T = 250$ K and at $T = 160$ K, the latter being below the transiton temperature (see next section). At 250 K, which is clearly the liquid phase, the disclination pairs tend to segregate to form grain boundaries which permeate the entire system. We have monitored the number of disclinations (ions with 5, 7 and 8 fold coordinates) as a function of temperature and our results are given in Figure 4. The data for the 216 ion system have been obtained from both cooling and heating runs. These calculations suggest a rapid decrease in the number of topological defects in the neighborhood of the transition region. Also note that at 250 K (see Figure 2) we can

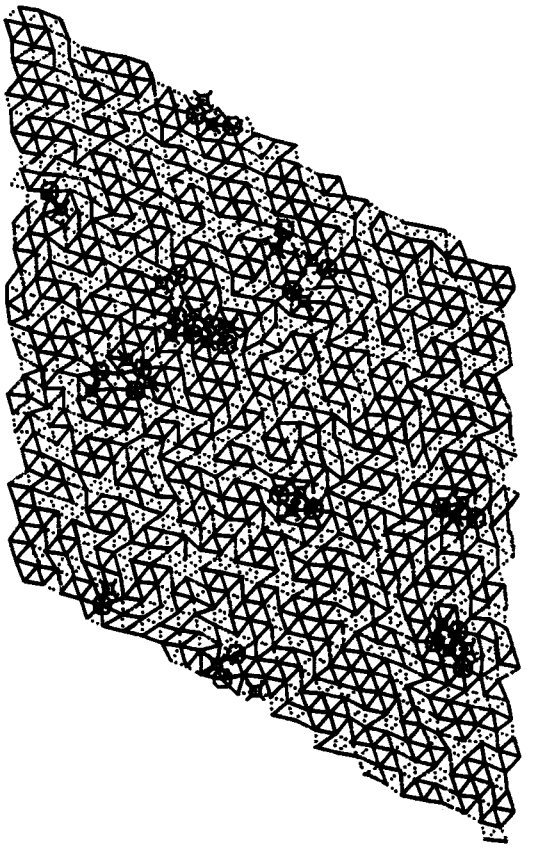

Figure 3 Picture of the 864 ion system at 160 K. Diamonds with 4 tails and circles mark the 5 and 7 fold coordinations, respectively. Yellow line indicates 3a, black indicates $\sqrt{7}$a and brown dots indicate 2a. (See Colour Plates)

identify some "free" disclinations, i.e., 5 and 7 fold coordinated atoms separated by more than one nearest neighbor bond, whereas at 160 K the disclinations appear to be "bound", i.e., separated by a nearest neighbor bond [30–32].

4 FREEZING REGION

Upon slowly cooling the system in steps of 10 K (with equilibration times >1 ns for the 864 ion system) from the liquid phase at 250 K, it appears to go through a freezing transition. Simulations have so far failed to give a definitive answer concerning the order of this transition (see detailed discussion in the next paragraph). However, the temperature range of the freezing transition and the emergence of a solid phase is adequately evidenced by our MD simulations. It may be noted that the heating and cooling runs for smaller systems agree fairly well. Details of our simulations are given below.

We have carried out extensive MD simulations in the microcanonical ensemble (EVN constant) with N = 96, 216 and 864 ions, respectively, at $140\,K < T < 290\,K$ to study the transition region. The linear behavior of T vs. E (since E is the

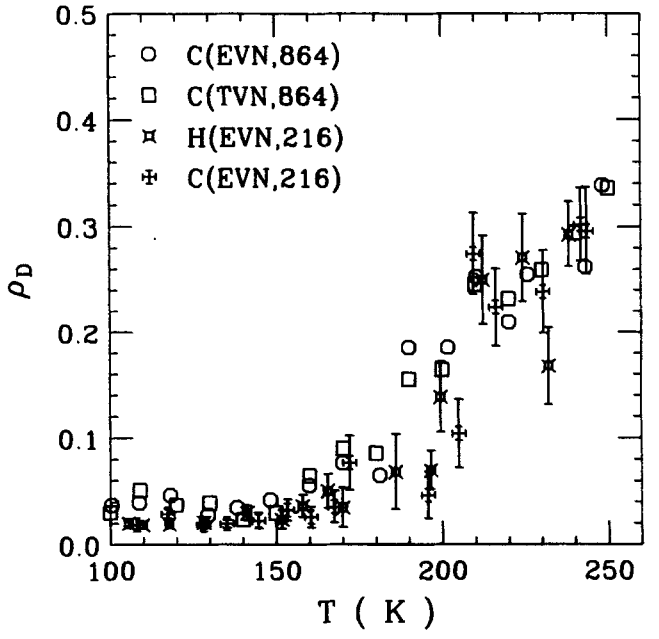

Figure 4 Number density of disclinations as a function of temperature for 216 ion system averaged over 30 samples. Observe the sharp rise in the density of disclinations at $T \approx 180\,K$.

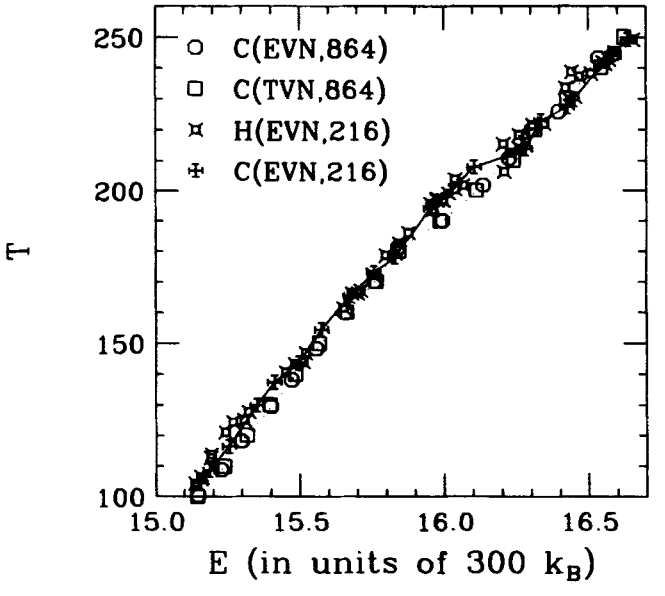

Figure 5 Plot of energy (E) versus temperature (T). The letter "C" denotes a cooling run while the letter "H" denotes a heating run. "EVN" and "TVN" imply microcanonical and canonical Nosé ensemble simulations, respectively, while the numbers 216 and 864 refer to the system sizes used for the data points reported. Observe the dependence of the E vs T curve on the system size at $180\,K \leq T \leq 215\,K$.

independent variable) reveals an abrupt change in the slope, dT/dE, in the liquid phase with $T > 200\,K$ to another in the region $180\,K < T < 200\,K$ and then back to a different slope for $T < 180\,K$ for the 864 ion system, thus suggesting a freezing region. The slope change occurs at higher temperatures for the smaller system sizes (see Figure 5). Let us define a temperture T_f where dT/dE changes significantly from its high temperature liquid value upon cooling. We find that T_f is sensitive to the system size, becoming progressively lower with increasing system size (see Figure 5) thereby suggesting that the freezing transition might be continuous. Our results for the 864 ion system suggest a freezing transition at $T_f - 180\,K$ in reasonable agreement with experimental findings on the melting temperature, typically claimed to be 165 K [12]. Larger system sizes and some sort of finite size scaling analysis are necessary for determining the precise phase transition temperature and the nature of the freezing transition. We have repeated our simulations using a canonical ensemble (TVN constant) via Nosé's method [29] for the largest system. The E versus T plots for the microcanonical and canonical ensembles are found to be in excellent agreement with each other (see Figure 5) for these cooling runs. It should be noted that equilibration times in the transition region are significantly longer than those away from it, being typically ~1.5 ns for the 864 ion system.

The freezing regime and the liquid to solid phase transition is further corroborated by the temperature dependence of the diffusion constant, D, obtained by plotting $\Sigma_{i=1}^{N}\langle|r_i(t) - r_i|^2\rangle/4N$ vs. t, N being the number of Rb ions, as shown in Figure 6. We find that D decreases from its liquid state value $\sim 0.5 \times 10^{-5}\,cm^2/sec$ at $T > 250\,K$ to a value less than $0.4 \times 10^{-6}\,cm^2/sec$ for $T \leq 150\,K$ (see Figure 6). These changes in D clearly suggest solid phase for

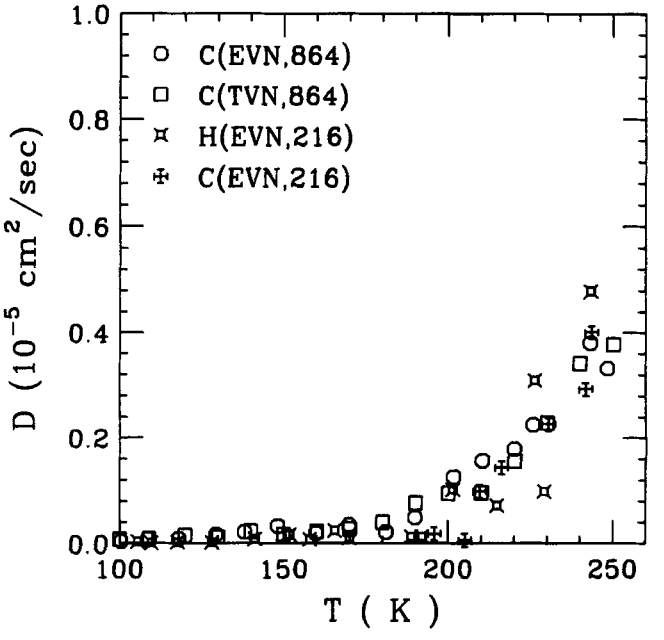

Figure 6 Plot of the diffusion constant D versus temperature T for the 864 ion system. Observe the sharp increase in D at $T \approx 180\,K$.

$T < 180$ K. We have also performed heating runs of the 216 ion system from the solid phase back up to the liquid phase. Our results are given in Figure 5 and reveal almost no hysteresis in the 216 ion system. The calculations have also been repeated for the larger 864 ion system where there is some indication of hysteresis. However, the equilibration times near the transition region are found to be so long, greater than ~1.5 ns, that we are not absolutely certain whether the system has reached equilibrium, in particular, for the larger system. We are therefore unable to definitively conclude whether the freezing transition is continuous or weakly first order, althought the smaller size system shows a continuous but sharp transition. More details of the transition region such as the temperature dependence of the orientational order parameter near the transition region are given elsewhere [19]. In fact, by monitoring the susceptibility associated with the orientational order parameter we find that the freezing temperature lies between 220 K and 230 K for the 216 ion system.

5 SOLID PHASE

5.1 *MD Simulations and Experiment*

The circularly averaged pair distribution function, g(r), describes the real space microstructure of a system depicting the local length scales present in the system, information which does not show up succinctly in the static structure factor. This is

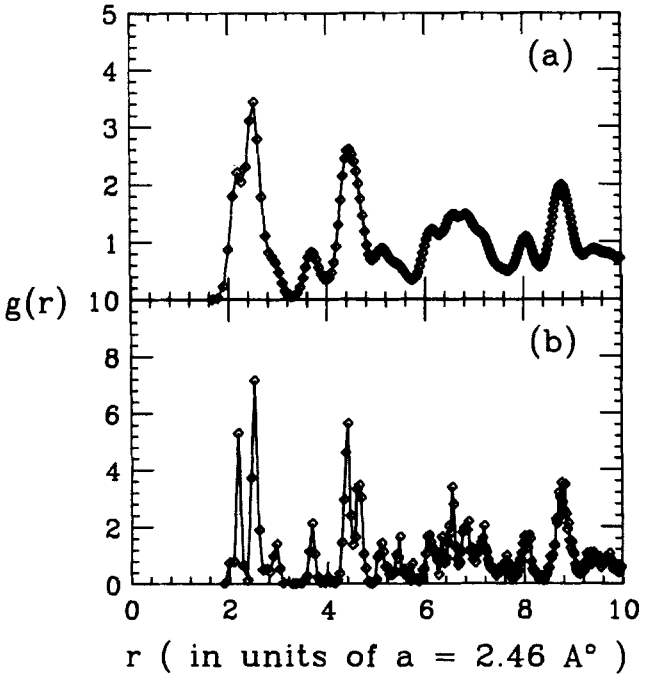

Figure 7 (top) The pair distribution function of the 864 ion system at T = 148 K. Note the main peak at $r \approx \sqrt{7}a$ and a weak peak at $r \approx 2a$. A shoulder at $r \approx 3a$ is barely visible. (bottom) The pair distribution function for the same system at 3 K. The peaks at $r \approx 2a$, $r \approx \sqrt{7}a$ and $r \approx 3a$ are clearly visible.

given in Figures 7a and b at two different temperatures, $T \simeq 148\,K$ and $T \simeq 3\,K$. Thermal vibrations freeze out at low temperatures and sharpen the pair distribution function. The solid phase is clearly characterized in Figures 7a, b with $g(r) \to 0$ at certain values of r. The pair distribution function exhibits a distinct three peak structure for $0 \leqslant r \leqslant 3.2a$ with two weak peaks at $r \approx 2a$ and at $r \approx 3a$ and one main peak at $r \approx \sqrt{7}a$. Observe that the liquid state pair distribution function (see Figure 1a) possesses well defined maxima's at $r > 3.2a$. These maxima's form sharp peaks at $r > 3.2a$ upon cooling to the solid phase (compare Figures 1a and 7a, b). Some of the structures in g(r) like those given here were also obtained by Plischke and Leckie [7] for the related system, CsC_{24}, for $50\,K \geqslant T \geqslant 300\,K$. However, their early work, paid little emphasis to the microstructure.

Let us first try to construct a periodic lattice structure exploiting the different local length scales present in this system as given in the pair distribution function (Figure 7b) by looking at the energetics. Simple calculations of energy/ion gives the following energies for the different possible commensurate structures: 9825 K $(2\times2\times2)$; 4476 K $(2\times3\times\sqrt{7})$; 3114 K $(\sqrt{7}\times\sqrt{7}\times\sqrt{7})$. Since the ions sit at the minimum of the corrugation potential, the corresponding energy/ion is the same for all those structures.

If we ignore the magnitudes of the peaks in the plot of g(r) vs. r in Figure 7b one would naturally guess that the correct low temperature lattice structure is triangular with sides of 2a, 3a, and $\sqrt{7}a$ (recall, $a = 2.46\,\text{Å}$) which would have given the correct RbC_{12} layer stoichiometry. However, the magnitudes of the peaks in Figure 7b are important and it turns out that the lattice structure is not simply $(2\times3\times\sqrt{7})$ but a combination of $(\sqrt{7}\times\sqrt{7}\times\sqrt{7}) \equiv (\sqrt{7}\times\sqrt{7})$, $(2\times2\times2) \equiv (2\times2)$ and $(2\times3\times\sqrt{7})$ structures. Our simulations suggest that Rb ions energetically prefer to approach a lattice structure with registered $(\sqrt{7}\times\sqrt{7})$ phase oriented at an angle (defined as the epitaxial angle) of 19.11° with respect to the graphite [10] axis, consistent with experimental observations. Therefore, although the $(2\times3\times\sqrt{7})$ structures give the correct layer density, the lower energy of the $(\sqrt{7}\times\sqrt{7})$ structures may favor the formation of the latter. However, the constraint of a fixed density hinders the formation of an *ordered* $(\sqrt{7}\times\sqrt{7})$ phase (which is expected to naturally occur for a layer stoichiometry of RbC_{14}, if it exists in nature) and instead leads to the formaiton of regions with (2×2) and $(2\times3\times\sqrt{7})$ structures. This picture is further corroborated by Figure 8. Alternatively, the lattice structure can be viewed as an ordered structure of plaquettes of $(\sqrt{7}\times\sqrt{7})$, each plaquette containing 7 Rb ions and is separated from the adjacent one by domain walls built of (2×2) and $(2\times3\times\sqrt{7})$ structures. The constraint of a fixed density leads to the formation of a few defects in this otherwise ordered system. Such a structure is described by Figure 8.

It may be noted that the ordered superlattice-like array of hexagonal plaquettes of $(\sqrt{7}\times\sqrt{7})$ structures in the top right of Figure 8 occur naturally in the equilibrated system. We will refer to the hexagonal plaquettes of $(\sqrt{7}\times\sqrt{7})$ structure containing 7 Rb ions as *nano-domains*. The intersection of three such plaquettes form a triangular plaquette of (2×2) structure. The walls between any two $(\sqrt{7}\times\sqrt{7})$ nandomains consist of $(2\times3\times\sqrt{7})$ triangular plaquettes which give rise to the peak near $r = 3a$ in Figure 7b. The wall regions should also give rise to a peak at $r = \sqrt{13}a = 3.6a$. Such a peak indeed appears as a fourth peak in Figure 7b. In fact, it is remarkable that this peak near 3.6a is also present in the liquid state at 250 K (Figure 1a) although broadened considerably. Even if Figure 8 suggests a tendency to form larger regions of $(\sqrt{7}\times\sqrt{7})$ structures, longer

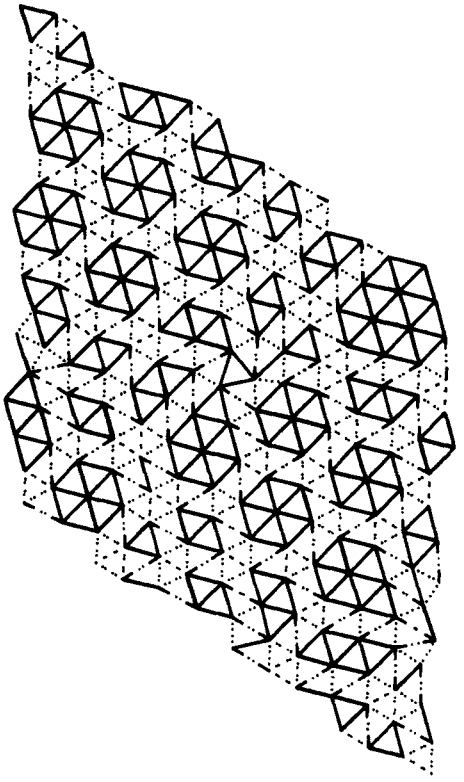

Figure 8 Picture of the 216 ion lattice at 3 K. Solid lines connect Rb ions $\approx \sqrt{7}a$ apart while dot-dash and dotted lines connect ions $\approx 3a$ and $\approx 2a$ apart. Observe the few large and few small regions of $\sqrt{7}a$ plaquettes which are necessary to satisfy the density constraint.

equilibration times do not lead to any phase separation and leave the structure of Figure 8 essentially unchanged.

It may be noted that our MD simulations give a picture very close to the one proposed by Zabel *et al.* [34] for RbC_{24}.

To compare our MD simulation structures with the X-ray diffraction measurements, we have computed the static structure factor $S(\mathbf{k})$ for the atomic postitions given in Figure 8. The structure factor for the solid phase is given in Figure 9 for both 216 and 864 ion systems. Recall that the structure factor for the liquid phase [6] at 250 K (see Figure 1b) shows the effect of corrugation with peaks at $\mathbf{k}$ values corresponding to the reciprocal lattice vectors of the graphite substrate. The dominant peak at $k = 1.19\,\text{Å}^{-1}$ corresponds to that of an incommensurate liquid. The solid phase $S(\mathbf{k})$ on the other hand shows three discernible peaks (exhibiting hexagonal symmetry) denoted as I_1, I_2 which sit on the perimeter of a circle and I_3. Thus, the *two dominant peaks (I_1 and I_2 have the same* $k = 1.21\,\text{Å}^{-1}$ but different orientational epitaxy angles ϕ_1 and ϕ_2, with $\phi_1 = 10.2°$ and $\phi_2 = 35.8°$ for the two peaks, respectively. The strengths of these two peaks are, respectively, 0.52 and 0.052. The third peak I_3 ($k = 1.40\,\text{Å}^{-1}$, $\phi_3 = 7.6°$) is extremely weak (strength 0.015), is not shown in Figure 9 and will not be discussed any further here.

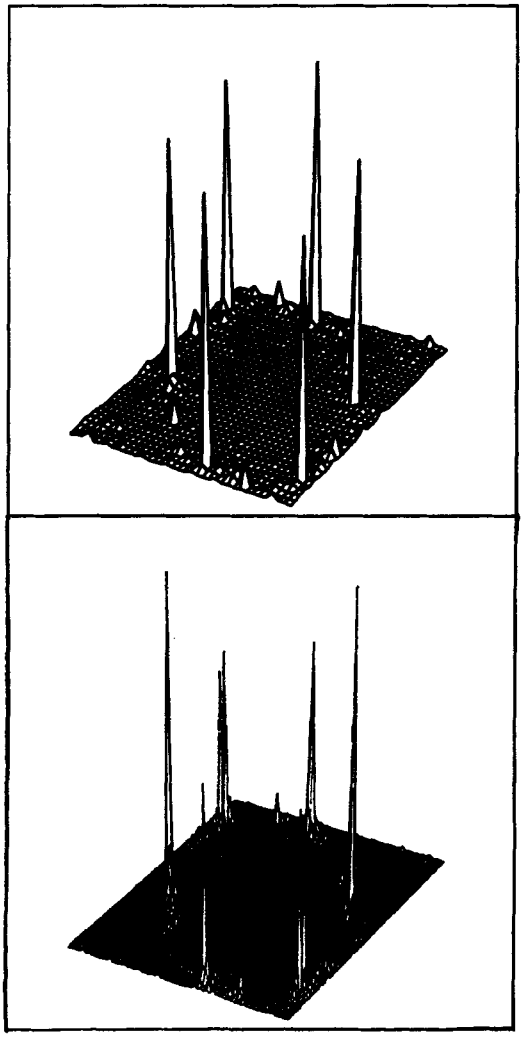

Figure 9 Plot of the static structure factor S(k) for the 216 ion (top) and 864 ion (bottom) system, respectively.

Clarke *et al.* [14] observed two peaks similar to I_1, I_2 in CsC_{24} (1 and 2 in their notation). They ascribed the origin of the peak I_2 to the coexistence of two different orientations of $(\sqrt{7} \times \sqrt{7})$ commensurate domains each containing about 30 Cs ions. Our MD simulations show only one orientation of domains, typically containing 7 Rb ions, thus indicating that the origin of the I_2 peak may be different from what was perceived earlier [14]. As we shall see later, this conjecture is also supported by the Periodic Domain Wall model to be introduced later in Section 5.2, and is consistent with the Ginzburg-Landau analysis [35]. For RbC_{24}, the dominant peak I_1 ($k = 1.23\,\text{Å}^{-1}$, $\phi_1 = 10.1°$), observed experimentally, is in excellent agreement with our MD results (see above). The lower intensity peak, I_2,

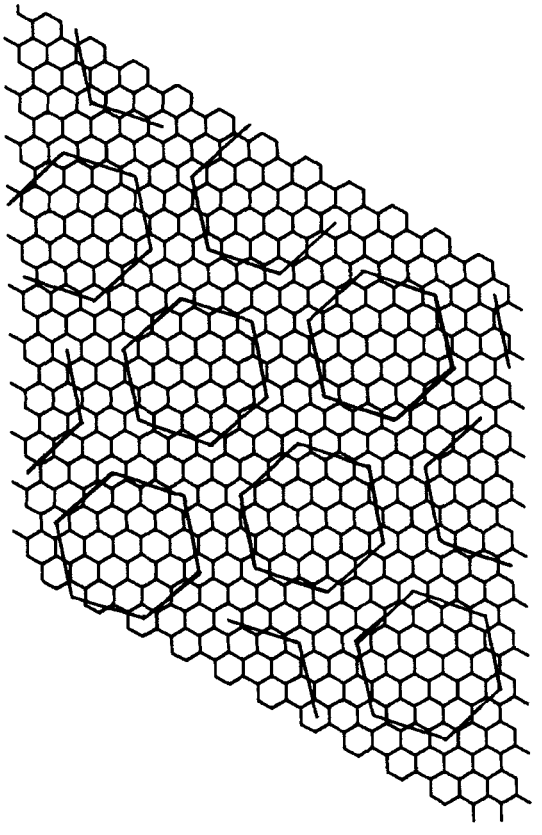

Figure 10 Picture of L = M = 1 Periodic Domain Wall model. Observe that the domain walls separating the nandomains (with 7 Rb ions which are $\sqrt{7}$a apart) have dimensions that are comparable to that of the domains.

for RbC_{24} was not discussed in Reference 14 but the corresponding angle ϕ_2 agrees very well with the diffraction results of Rousseaux *et al.* [36].

5.2 *Interpretation of S(k) based on Periodic Domain Wall Model*

To obtain a general understanding of the origin of the two peak, I_1 and I_2 discussed above, we propose a *Periodic Domain Wall (PDW) Model* which consists of periodic arrays of commensurate $(\sqrt{7} \times \sqrt{7})$ domains of total width 2L (all of the same orientation) interspersed by domain walls of width M (see Figure 10). The domain walls consist of $(2 \times 3 \times \sqrt{7})$ regions. The regions where the three domains meet consist of triangular arrays of (2×2) structure. In this model, where all the Rb ions sit at the minima of the one particle corrugation potential, one goes from the commensurate $(\sqrt{7} \times \sqrt{7})$ structure (M = 0, arbitrary L), corresponding to a stoichiometry of XC_{14}, to the commensurate (2×2) structure (L = 0, arbitrary M), corresponding to XC_8, where X stands for alkali-metal. Thus, the layer density is determined by (L, M). For arbitrary (L, M) the superlattice unit cell is obtained by joining the centers of the $(\sqrt{7} \times \sqrt{7})$ domains. The unit cell vectors

of the PDW model are given by

$$\mathbf{A} = 2(2L+M)\mathbf{a} + L\mathbf{b}, \tag{5.5}$$

and

$$\mathbf{B} = -L\mathbf{a} + (5L+2M)\mathbf{b}, \tag{5.6}$$

where $\mathbf{a} \equiv a\mathbf{x}$ and $\mathbf{b} \equiv (a/2)\mathbf{x} + (\sqrt{3}a/2)\mathbf{y}$, where $\mathbf{x}$ is a unit vector along the (10) direction of graphite in real space and $\mathbf{y}$ is a unit vector perpendicular to $\mathbf{a}$ in a right-handed coordinate frame. The corresponding reciprocal lattice vactors are given by

$$K_{Ax} = 2\pi(5L+2M)/a(21L^2+18LM+4M^2), \tag{5.7}$$

$$K_{Ay} = \{-(3L+2M)/(5L+2M)\sqrt{3}\}K_{Ax}, \tag{5.8}$$

and

$$K_{Bx} = -2\pi L/a(21L^2+18LM+4M^2), \tag{5.9}$$

$$K_{By} = -\{(9L+4M)/L\sqrt{2}\}K_{Bx}. \tag{5.10}$$

Our MD simulations suggest that RbC_{24} can be well described by the *PDW model* with $L = M = 1$, which corresponds to a stoichiometry of $RbC_{24.57}$, i.e., a planar stoichiometry of $RbC_{12.29}$ (see Table 1). The RbC_{12} lattice can then be regarded as an $L = M = 1$ system with a small number of extra Rb ions, i.e., defects, to restore the correct stoichiometry. As mentioned in Section 5.1, Clarke *et al.* [13] reported only a dominant peak I_1 ($k = 1.23$ Å, $\phi_1 = 10.1°$) for RbC_{24}. The dominant peak I_1 is in excellent agreement with our PDW model results, which gives ($k = 1.19$ Å, $\phi_1 = 11.5°$). We found that I_2 has the same k value and $\phi_2 = 33.3°$, the intensities of the two peaks being 0.573 and 0.137, respectively (see Table 1). We have obtained the ground state structure of $RbC_{24.57}$ [13] using MD simulations. We do indeed find a PDW solid with $L = M = 1$ with intensities I_1 and I_2, respectively, to be 0.702 and 0.1444. The differences between the values of $I_1$and I_2 obtained via the PDW model calculations and those obtained via MD calculations stem from the fact that the Rb ions do not sit at the bottom of the corrugation potential in the MD study while they do so in the PDW picture.

We also find that the CsC_{24} results of Clarke *et al.* [14] can be approximated by an $L = 2$, $M = 1$ PDW model which corresponds to a layer stoichiometry of $CsC_{13.05}$. Our calculations of the structure factor S(k) for this model give $K = 1.15$ Å^{-1} and $\phi_1 = 14.46°$, $\phi_2 = 27.63°$, in excellent agreement with corresponding experimentally measured values of 1.16 Å^{-1}, 14.5° and 28°, respectively,

Table 1 $M = 1$

L	ϕ_1	ϕ_2	I_1	I_2/I_1	$\lvert k \rvert$	y (in XC_y Stage-2)
1	11.52	33.31	0.573	0.239	1.19	24.57
2	14.46	27.63	0.568	0.253	1.15	26.10
3	15.75	25.18	0.570	0.257	1.14	26.70
∞	19.11	19.11	1.0	—	1.11	28.00
Molecular Dynamics Simulation results						
—	10.2	35.8	0.520	0.100	1.21	24.00

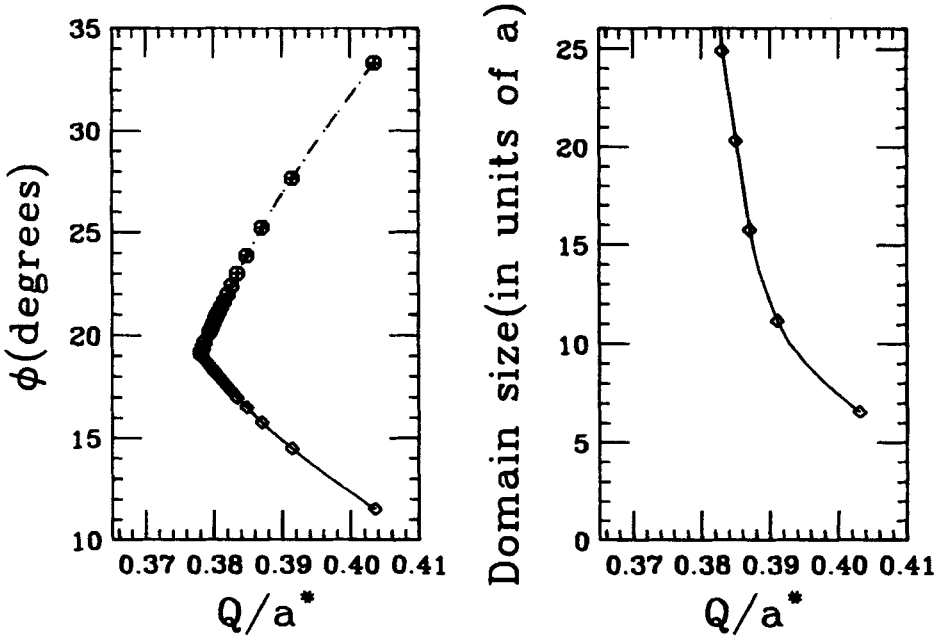

Figure 11 (Left) The top curve gives the orientational epitaxy angle ϕ_2 of peak I_2 while the bottom curve gives the orientational epitaxy angle ϕ_1 of peak I_1 as a function of the layer density. (Right) gives the domain size as a function of the layer density [1]. Observe that the domain size grows to ∞ as layer stoichiometry approaches RbC_{14}.

for the stage 2 CsC_{24} (see Clarke *et al.* in Reference 14). We find the intensities for the peaks I_1 and I_2 to be 0.568 and 0.144, respectively, i.e., $I_2/I_1 = 0.253$. This ratio compares favorably with the experimental ratio of 0.21 obtained by Winokur and Clarke for a stage-3 CsC_{36} in reference 14.

The dependence of the epitaxy angles ϕ_1 and ϕ_2 and of the domain size on the concentration are described by Figure 11. Within PDW model as $L \to \infty$, the angles ϕ_1 and ϕ_2, which give the positions of the peaks I_1 and I_2 approach 19.11°. In fact, we find by actual calculation that the epitaxy angles ϕ_1 and ϕ_2 satisfy the relation

$$\sin\phi_2 = \sqrt{3}\,.\,\sin(30° - \phi_1), \tag{5.11}$$

for the PDW model with $M = 1$ and arbitrary L. These two peaks merge with each other for the commensurate $(\sqrt{7} \times \sqrt{7})$ case. Thus, the restoration of a fully commensurate lattice structure without any domain walls leads to only one peak. These findings confirm that the appearance of the peak I_2 originally noted by Clarke *et al.* [14] is unrelated to the presence of domains of commensurate $(\sqrt{7} \times \sqrt{7})$ regions with two different orientations, $\pm 19.11°$ (see Figure 11). Indeed, such configurations, which generally require the Rb ions to be located closer than a distance 2a in the regions between the domain walls (if we insist on the layer density of RbC_{12}) are energetically unfavorable in view of the strongly repulsive two body potential between these ions.

6 DISCUSSION

This paper presents extensive Molecular Dynamics calculations on the structural properties of RbC_{24} stage 2 GIC's. We have used a screened Coulomb interaction between the Rb ions and the graphite layer is approximated using a one body corrugation potential following Chen *et al.* [6] We find that RbC_{24}, a stage 2 alkali metal GIC, behaves as a highly corrugation modulated liquid at $300\,K \geq T \geq 200\,K$ with three distinct local length scales, $r \sim 2a$, $\sqrt{7}a$ and $3a$, where $a = 2.46\,Å$. The liquid state calculations agree with the earlier results on the structure factor S(k) of Chen *et al.* [6] We observe that the "liquid state lattice" includes many disclinations, both bound and free (see Figure 2).

We find that this system undergoes a freezing transition at $200\,K \leq T_f \leq 240\,K$. The transition is indicated via a distinct change in slope dT/dE in the transition region compared to the slopes at higher and lower temperatures (Figure 5). It is also signalled by a rapid increase in the diffusion rate (Figure 6), and also a rapid increase in the density of topological defects (Figure 4). The transition region is characterized by long equilibration times, typically in excess of 1.5 ns for the 864 ion system.

In the solid phase, we find that the lattice exhibits well defined hexagonal nano-domains of $(\sqrt{7} \times \sqrt{7})$ structure, containing 7 Rb ions in each nano-domain (Figure 8). The nano-domains are separated from each other by thick domain walls made up of $(2 \times 3 \times \sqrt{7})$ and (2×2) triangular plaquettes (see Figure 10). The intersection of three nano-domains form a triangular plaquette of (2×2) structure containing 3 Rb ions.

Our studies indicate that the domains and the domain walls possess comparable length scales in the RbC_{24} system, unlike what has been envisioned earlier. The structure factor S(k), corresponding to this low temperature lattice structure, is in excellent agreement with the measurements of Clarke *et al.* [14] and Rousseaux *et al.* [36]. Our simulation results suggest a Periodic Domain Wall model for describing the solid state structure of RbC_{24} and CsC_{24} GIC's. In fact, we explicitly show that the $L = M = 1$ PDW model (Figure 10) adequately describes the structure factor of RbC_{24} while the $L = 2$, $M = 1$ model possesses some of the crucial features of the structure factor of stage-2 CsC_{24} and stage-3 CsC_{36} described by Clarke *et al.* [14].

Acknowledgements

We have benefited from useful conversations with several colleagues during the course of this work, especially Drs. Zhi-Xiong Cai, Sue Coppersmith, Professors Andrei Talapov, John Ray, W.A. Steele, Kathy Strandburg and Michael Thorpe. This work has been supported inpart by NSF DMR MRG grant 89-03579, NSF DMR grant 90-24955 and by an AURI grant from Michigan State University.

References

[1] H. Zabel and S.A. Solin eds. Graphite Intercalation Compounds, Vol. 1: Statics and Dynamics. Springer Series on Topics in Current Physics, Springer, Berlin (1989).

[2] See for example F.F. Abraham, "Computational statistical mechanics: methodology, applications and supercomputing", Adv. Phys., **35**, 1 (1986); see also Dynamics of Gas-Surface Interactions, eds. G. Benedek and U. Valbusa, Springer, Berlin (1982).

[3] As for instance in K.G. Huang, D. Gibbs, D.M. Zehner, A.R. Sandy and S.G.J.Mochrie, "Phase behavior of the Au(111) surface: discommensurations and kinks", *Phys. Rev. Lett.*, **65,** 3313 (1990).
[4] S.A. Solin and H. Zabel, "Physics of ternary graphite intercalation compounds", *Adv. Phys.*, **37,** 87 (1988).
[5] H. Ehrenreich and D. Turnbull eds. Solid State Physics, Vol 40, Academic, Orlando (1987).
[6] Z.M. Chen, O.A. Karim and B.M. Pettitt, "A theory of the interionic structure of graphite intercalation synthetic metals: Variations with respect to interactions and state", *J. Chem. Phys.*, **89,** 1042 (1988) and Z.M. Chen, T. Cagin and B.M. Pettitt, "Structure of atomic and diatomic graphite intercalation compounds: simulations and integral equations" (unpublished).
[7] M. Plischke and W.D. Leckie, "Temperature dependence of the pair correlation functions in an inhomogenouse liquid: application to $C_{24}Cs$", *Can. J. Phys.*, **60,** 1139 (1982).
[8] S.C. Moss, G.Reiter, J.L. Robertson, C. Thompson, J.D. Fan and K. Ohshima, "X-ray determination of the substrate modulation potential for a two-dimensional Rb liquid on graphite", *Phys. Rev. Lett.*, **57,** 3191 (1986).
[9] P.B. Visscher and L.M. Falicov, "Dieletric screening in a layered electron gas", *Phys. Rev.*, **B3,** 2541 (1971).
[10] J.D. Fan, O.A. Karim, G Reiter and S.C. Moss, "Molecular Dynamics study of the temperature-dependent two-dimensional Rb liquid in graphite", *Phys. Rev.*, **B39,** 6111 (1989).
[11] G. Reiter and S.C. Moss, "X-ray scattering from a two-dimensional liquid modulated by its periodic host", *Phys. Rev.*, **B33,** 7209 (1986).
[12] J.D. Fan, G. Reiter and S.C. Moss, "Dynamics of a 2D liquid on a periodic substrate: Rb on graphite", *Phys. Rev. Lett.*, **64,** 188 (1990).
[13] H. Seong, S. Sen, T. Cagin and S.D. Mahanti, "Domains and domain walls in graphite intercalation compounds", *Phys. Rev.*, **B45** (Rapid communication), 8841 (1992).
[14] R. Clarke, J.N. Gray, H. Homma and M.J. Winokur, "Evidence for discommensurations in graphite intercalation compounds", *Phys. Rev. Lett.*, **47,** 1407 (1981).
[15] M.J. Winokur and R. Clarke, "Pinned incommensurate structure of Cesium intercalated graphite", *Phys. Rev. Lett.*, **54,** 811 (1985).
[16] M.K. Winokur, PhD Thesis, University of Michigan, Ann Arbor (1985).
[17] S.C.Moss and R. Moret, "Structural properties and phase transitions", in ref. 1.
[18] M.O. Robbins, K. Kremer and G.S.Grest, "Phase diagram and dynamics of Yukawa systems", *J. Chem. Phys.*, **88,** 3286 (1988).
[19] H. Seong, S.D. Mahanti, S. Sen and T. Cagin, "Melting of a repulsive screened Coulomb system in 2D-effect of corrugation", *Phys. Rev.*, **B46,** 8748 (1992) (submitted).
[20] E. Vives and P-A. Lindgard, "Substrate influence on two dimensional solids and liquids: A Monte Carlo simulation study", *Phys. Rev.*, **B44,** 1318 (1991).
[21] J. Krumhansl and J.R. Schrieffer, "Dynamics and statistical mechanics of a one-dimensional model Hamiltonian for structural phase transitions", *Phys. Rev.*, **B11,** 3535 (1975).
[22] W.C. Kerr and A.R. Bishop, "Dynamics of structural phase transitions in highly anisotropic systems", *Phys. Rev.*, **B34,** 6295 (1986).
[23] S. Sen, N. Mousseau and G.T. Overney, "Onset of avalanches in granular media", *Phys. Rev. Lett.* (submitted).
[24] P. Bak, "Mode locking and chaos in sliding charge density wave systems", in Charge density waves in solids, eds. G. Hutiray and J. Solyom, Springer, Berlin (1985).
[25] V. Pokrovskii and A. Talapov, "A theory of two-dimensional incommen-surate crystals", *Sov. Phys. JETP.*, **51,** 134 (1980) and **51,** 654 (1980) (E).
[26] S. Coppersmith, D.S. Fisher, B.I. Halperin, P.A. Lee and W.F. Brinkman, "Dislocations and the commensurate-incommensurate transition in two-dimension", *Phys. Rev. Lett.*, **46,** 549 (1982).
[27] Z-X. Cai and S.D. Mahanti, "Lattice gas melting of two-dimensional alloys: application to ternary graphite intercalation compounds", *Phys. Rev.*, **B36,** 6928 (1987).
[28] M.P. Allen and D.J. Tildesley, Computer Simulation of Liquids, Clarendon, Oxford (1987), see Appendix E, p. 340.
[29] S. Nose, "A unified formulation of constant temperature Molecular Dynamics", *J. Chem. Phys.*, **52,** 255 (1984).
[30] D.R. Nelson, "Defect-mediated phase transitions", in Phase Transitions and Critical Phenomena, Vol 7, eds. C. Domb and J.L. Lebowitz, Academic, London (1983).
[31] B.I. Halperin and D.R. Nelson, "Theory of two-dimensional melting", *Phys. Rev. Lett.*, **41,** 121 (1978) and *Phys. Rev. Lett.*, **41,** 519 (1978) (E).
[32] D.R. Nelson and B.I. Halperin, "Dislocation mediated melting in two-dimensions", *Phys. Rev.*, **B19,** 2457 (1979).

[33] **C.A. Rogers, Packing and Covering, Cambridge, New York (1964).**
[34] H. Zabel, S.E. Hardcastle, D.A. Neumann, M. Suzuki and A. Magerl, "Dynamics of two-dimensional melting on a periodic substrate", *Phys. Rev. Lett.*, **57,** 2041 (1986).
[35] Y. Yamada and I. Naiki, "Discommensuration structure of mass density waves in higher graphite intercalation compounds", *J. Phys. Soc. Jpn.*, **51,** 2174 (1982).
[36] F. Rousseaux, R. Moret, D. Guerard and P. Lagrange, *Phys. Rev.*, **B42,** n25 (1990); F. Rousseaux *et al. Synth. Met.*, **12,** 45 (1985).